Chapter 2

Experimental Methods and Theoretical Models

The detection and identification of particles produced by nuclear reactions are critical tools for studying several aspects of nuclear processes. The particle's mass, charge, kinetic energy, and emission angle are crucial elements to be found for their identification. If the outgoing channel of a nuclear reaction consists of two particles, the kinematic details of the process can be reconstructed by detecting and identifying one of the particles. But this situation becomes complex when three particles are involved in the final kinetic energy distribution. Reactions accompanied by breakup are the latter type of complexity. To implement the proper study of the breakup mechanism, we need to carefully understand the generation and detection of these particles. This study of breakup nuclear reactions involves the production of particles, and their acceleration which is attended by detection, electronic setup, and data acquisition system. A brief discussion of each of these components is presented.

2.1 Production and Acceleration of particle:

The study of low energy nuclear reactions typically includes projectiles with energies ~10 MeV/ nucleon. This much energy can be attained with help of accelerators. In India, several accelerators are installed to track nuclear research. The research work presented in the thesis was executed at Inter University Accelerator Centre (IUAC), 15 UD pelletron facility, New Delhi, and BARC-TIFR, 14 UD pelletron facility, Mumbai. Both of these are tandem Van De Graff electrostatic accelerators. A typical schematic pelletron accelerator is shown in figure 2.1. The very first component of the pelletron is the ion source 'SNICS (Source of Negative Ion by Cesium Sputtering)' at top of the pelletron tower where negative ions are generated from the source and pre-accelerated $E_0 \approx 250$ KeV. With the guidance of the injector magnet, a typical mass of selected ions is injected into a sturdy electric field inside an accelerator tank stuffed with insulating SF_6. This beam is accelerated with energy $eV_{T,}$ where V_T is terminal voltage. Towards high terminal voltage in million volts at the center of the tank. The terminal voltage for IUAC pelletron is 15V and for BARC-TIFR pelletron is 14 V. The high electric field is achieved by utilizing steel pellets to maintain uniform charging and is mutually separated from the insulator. Therefore these accelerators are named *Pelletron accelerators*. At the terminal, a thin carbon foil of thickness ~5μg/cm^2 or a small volume of gas is used as a stripper and this is adjusted such that it strips off some electrons from each negative ion and thus converts them into positive ions. Since the terminal is staying at a positive potential, the positive ion face repulsion

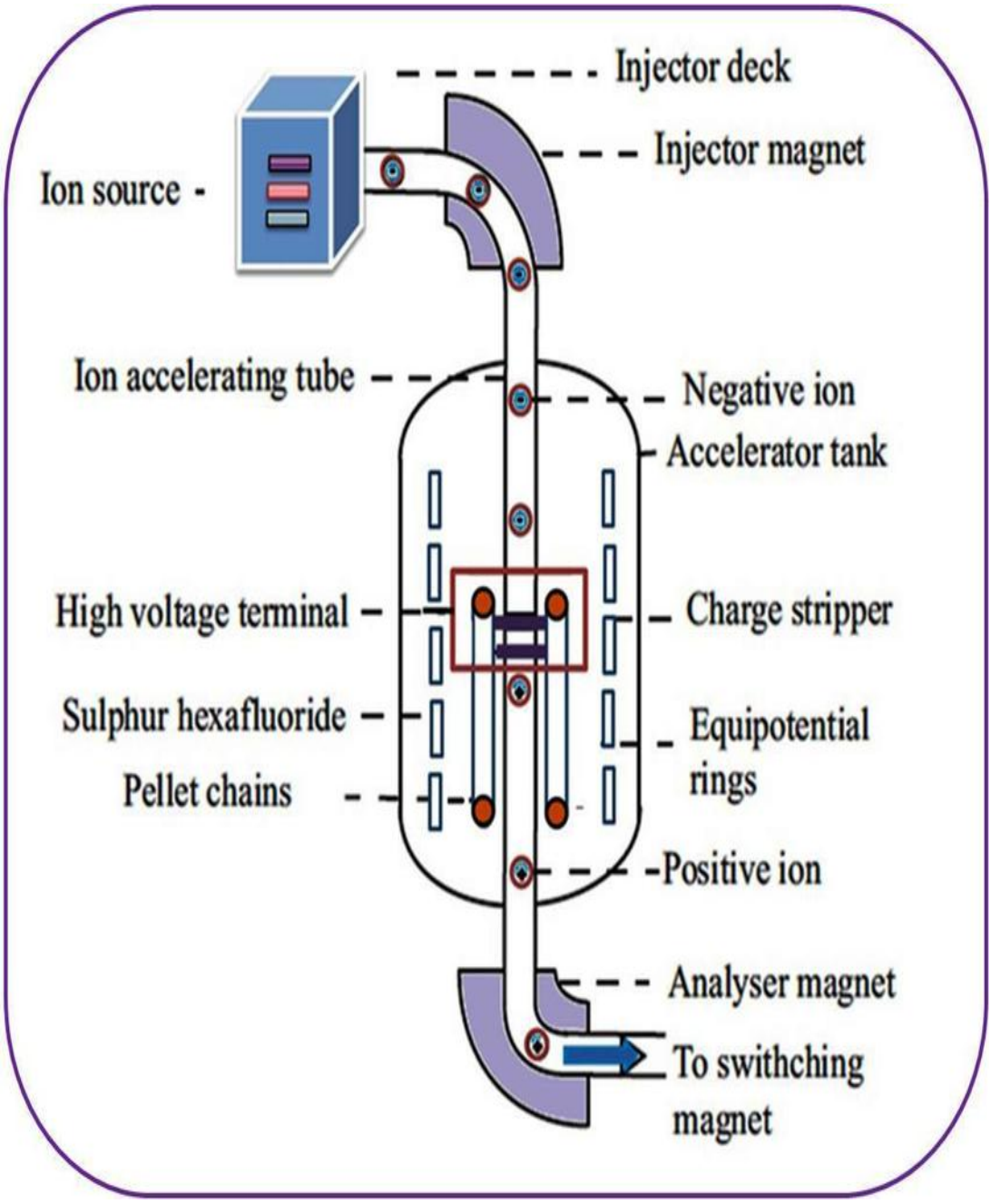

Figure 2.1: *Schematic block diagram of a typical pellletron accelerator tank [1]*

away from this and accelerated to the ground. Thus the energy achieved by the q charge particle becomes qV_T. Thus the final energy becomes a total sum of

$$E= [E0 + (q+1)\ V_T]\ MeV \qquad (2.1)$$

At the end of the tube analyzing magnet is established to keep analyzing a specific charge and energy selection. At the last, taking assistance of a switching magnet, the beam of ions is monitored to a specific beam line like 'General Purpose Scattering Chamber (GPSC)' or 'Indian National Gamma Array (INGA)' or 'Gamma Detector Array (GDA)', or towards the material science line or biology science, etc. The measurement carried out in the presented thesis were taken in GPSC.

2.2 Target Fabrication

The target of appropriate thickness plays a very crucial and centered role in experimental nuclear physics. Depending on the purpose the thickness may vary and needs special attention in terms of energy loss. In nuclear reaction experiments, thin targets are of very high importance. Along with the thickness, the factors like uniformity in thickness, sustainability against high energy beams, isotopic purity, good tensile strength, etc. are of core importance and should be taken care of properly while fabricating the targets. The purpose is fulfilled by using a high vacuum (HV) evaporator chamber, an ultra- high vacuum (UHV) evaporator chamber, tabular furnace. Physical vapor deposition (PVD) technique was exploited with e-gun evaporation. The HV setup is accommodating a diffusion pump along with a liquid nitrogen trapper for oil droplets to

achieve a pressure of 1.5x 10^{-8} mbar. The UHV evaporator is facilitated by a turbo molecular pump and cryo-pump to achieve a pressure of ~ 10^{-11} torr. The multi-pocket advantage is always there so that the sequential deposition of required material can always be fulfilled. The cryo pump helps towards reducing more contaminants like carbon. Both the evaporator units possess a piezoelectric crystal based thickness monitor 23 cm away from source. The schematic diagram of both chambers can be found in T. Banerjee et al. [2]. The following steps are adopted for fabricating a typical nuclear reaction target.

(a) Natural carbon baking: The parting reagent Potassium chloride (Kcl), was used as a parting agent and was brought into the frame in form of a pellet. After the thorough cleaning of the HV chamber and attaining the requisite pressure the deposition started. At a distance of 21 c.m. the glass substrate holder was placed over which the film was to be deposited. The multi pocket facility gives the advantage to deposit different materials in a single run. Kcl having very low lattice energy was a good choice for parting reagent that was deposited with the fixed rate of 0.4 Å/s till the thickness monitor indicated the 100 nm thickness. The natural carbon also in form of pellets and was exposed to an e-beam at 0.1 Å/s to obtain a thickness of 22μg/cm^2. After the deposition, the chamber was in the cooling process for almost 8 hours. Due to deposition, the thin films are under stress so to contrive, annealing of deposited is done at 250°C for 1 hour in an inert argon environment and allowed for argon as well natural cooling. This leads to post-deposition of the material in the sense of recovery, recrystallization, or chemical reaction depending on the temperature and time.

(b) Molybdenum deposition: : In the ultra-high vacuum chamber where the vacuum can be achieved up to the order 10^{-11} torr, the annealed carbon slabs were loaded to furnish Mo deposition at some prominent distance. There were several trials with natural Molybdenum to check out the texture, sustainability, and floating properties of the film which has to be compromised with the availability of pure raw material. After optimizing the parameters with natural Mo the UHV chamber is cleaned thoroughly for isotopic film deposition. The pure isotopes were supplied from Oak Ridge Laboratory, USA. The isotope ^{92}Mo was in rod form of 100 mg weight so just accumulated and was put in the crucible. The ^{100}Mo was in form of powder, molded to a pellet of 3mm diameter to secure minimum loss of the material. ORL claims 99.05% enrichment of ^{100}Mo of 100mg amount. The pressure was maintained at the order of 10^{-7} torr during the deposition. The substrate was kept at 7 cm distance from the source and the crystal based thickness monitor was at a distance of 21 cm from the source. After attaining a pressure of 10^{-11} torr the deposition of ^{92}Mo was done at a current of 170 mA/A with a rate of 0.1 Å/s till the thickness of 211 nm. The same parameters were fixed for ^{100}Mo deposition and also for another set of carbon deposited slabs to achieve a thickness of 297 nm. The chamber was allowed to cool for 8-10 hours after each run of isotopes.

(c) Annealing: The thin films were allowed to go for annealing at 250°C for 1 hour in an argon environment and undergo natural cooling. This process supported post growth of the films. As described earlier this leads to post-deposition of the material in the sense of recovery, recrystallization, or chemical reaction depending on the temperature and time.

Figure 2.2: *Deposition of ^{92}Mo during the run and internal view of the chamber after deposition respectively.*

(d) Target Preparation: The isotopes were floating in lukewarm deionized water and were taken carefully on the target frame holder. We could make 20 targets of 20μg/cm^2 thicken carbon backed ^{92} Mo of thickness 217 μg/cm^2 and 16 targets of 20μg/cm^2 thicken carbon backed ^{100}Mo isotopes of thickness 305 μg/cm^2. One of the blank slab was there in each run to have the isotope deposition and afterward it is used to measure the thickness of the deposited film using a stylus profilometer. We fabricated Mo isotopes thin film using carbon backing of approximately 20 μg/cm^2 and deposited Mo isotopes sequentially over it in different runs [3].

Figure 2.3: *Floating off the thin film and taking on SS target frame for target fabrication.*

2.3 Interaction of charged particle with matter:

When a charged particle hits the detector, it is primarily interacting with the last shell electrons of atoms of the detector's material via the Coulomb field. The particle will transmit its energy to the atom as it passes through the material. Because electromagnetic interactions have a great range, it is not essential for a light or heavy charged particle to collide directly with an atom. Further due to this interaction, the energetic charge particle can either excite the electron or remove it from the shell and thus result in a loss of energy. The basic principle of energy loss in semiconductor detectors (ΔE-E telescope configuration here) may be given by the Bethe-Bloch formula [4]. The formula calculates loss of energy of an incoming entity travelling in a detector correctly as $-\frac{dE}{dx} = \frac{MZ^2}{E}$, where E is incident energy, M and Z are mass and atomic number respectively of the incoming particle. Less energetic and more massive particles will deposit more energy. In the telescope configuration, ΔE is the thinner detector where less energy is deposited by incoming particles, and just after this thicker E is present where all remaining energy is dumped. A standard plot between ΔE vs. E_{Total} provides different bands of energy loss for different mass particles and thus helps to distinguish the fragments involved in the reaction. A schematic demonstration of the telescope is given in figure 2.4

In the modern era, mostly semiconductor detectors are found suitable in detection techniques due to the following reasons:

(i) the narrow band gap (~1 eV) makes the generation of electron-hole pairs easier

(ii) they are compact in size

The semiconductor detector is reversed biased p-n junction diode. In this particular operation, depletion depth gets increased with bias voltage and thus region becomes charge free. Now when an energetic charge particle enters this region, creates electron-hole pairs, a drift of these charge carriers produces an electrical signal.

The semiconductor detection system utilized in our experiment are silicon surface barrier detectors. To create the p-n junction, an n-type silicon wafer is oxidized on one side and then coated with a thin coating of gold. The characteristics of the surface barrier are greatly influenced by the little oxidation of the gold layer before evaporation. After that, the junction is encased in an insulating ring with metalized surfaces for ohmic connections. Because the barrier is produced at the crystal's surface, detectors made in this manner are known as silicon surface barrier detectors (SSB). SSBs of varied thickness and depletion regions may be manufactured.

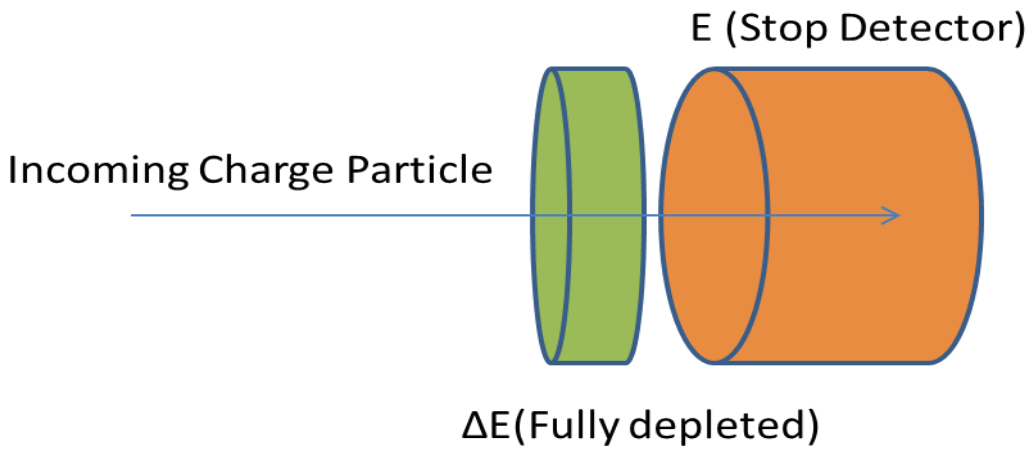

Figure 2.4: *Schematic illusion of ΔE-E telescope detector setup. ΔE is the thinner solid state/gas detector where less energy is deposited by incoming particles and just after this thicker E, solid state detector is present where all remaining energy is dumped by particles.*

2.4 Electronics for processing of signals and Data Acquisition:

A high energy incident beam of ion interacts with the target attached to the target ladder and after the reaction events are measured by the detector. Due to the specific volume of detectors and various interaction procedures of different particles, each energy signal which is deposited in the detector can be correlated and scaled. Those events thus we can record using proper electronics. Primary signals produced are small and need amplification. From each telescope detector, the preamplifier signals are fed to amplifiers using coaxial cables. These amplifiers shape the signal using inbuilt CR & RC circuits and thus amplify the signal. Generally, an electrical signal generated by a detector can be processed for two information namely energy and timing. The timing signals produced by ΔE are connected to the preamplifier and this fast output is fed further to Timing Filter Amplifier. All Timing filter signals from all ΔE detectors are fed to the Constant Fraction Discriminator (CFD) with a delay cable to have a delay signal. This delay output stops the signal and the corresponding start signal is taken from the main trigger for Time to Digital Converter (TDC). Timing signals from CFD via logic OR gate are fed to Gate and Delay Generator (GDG) where the main gate is built and given as master strobe to ADC. ADC converts all analog signals to digital [5]. Afterward, ADC signals are sent to the data acquisition system with help of BUS. A schematic picture is given below in the figure 2.5. A very popular data acquisition system is 'LAMPS (Linux Advanced Multi Parameter System)' [6], which can be used offline also.

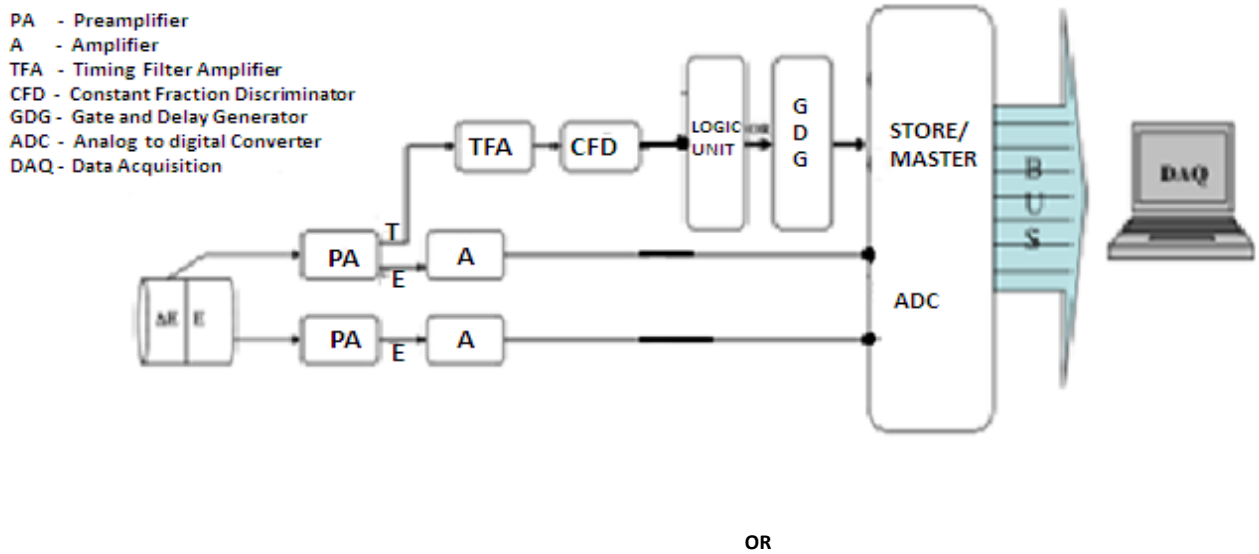

Figure 2.5: *Schematic block diagram of electronic setup corresponding to the experimental arrangement in the thesis.*

2.5 Theoretical models for nuclear reactions:

2.5.1 Optical Model and Optical Potential:

The nuclear reaction incidents like nucleon-nucleon or nucleon-nucleus interactions are very complicated to draw into a complete model. Feshbach, Porter, and Weisskopf proposed the Optical Model in 1954 in which this complication was simplified by considering two body interactions between incident and target nucleus. This model suggests that incident particle encounters an average complex potential while interacting with a target nucleus [7, 8]. An interplay of incoming nucleons with target nucleus can be compared to light transmission through a cloudy refractive medium. It was also known as the 'cloudy crystal ball model'.

According to the model considered, elastic scattering can be thought to play the role of refraction phenomenon and all channels other than elastic as absorption process. As a result, the optical potential is divided into dual parts: real and imaginary. Where real component causes elastic scattering and imaginary portion causes absorption from an elastic channel. This was regarded as a complex potential for ascribing possibility of non-elastic scattering into imaginary part. The optical model has two features. The first is connected to the fundamental one, which is concerned with nucleon-nucleon interactions. The second part is the phenomenological aspect, in which parameters must be carefully set and can be modified for obtaining a justified result with experimental results. The second approach was used in this work for optical model analysis of elastic scattering angular distributions.

Sum of Coulomb $V_C(r)$ and nuclear $V_N(r)$ potentials describes total potential.

$$V(r) = V_C(r) + V_N(r) \tag{2.2}$$

The Coulomb potential can be considered in the following form,

$$Vc(r) = Zp\ Z_T\ e^2 \begin{cases} \frac{1}{r} & r \geq Rc \\ \left(\frac{3}{2} - \frac{r}{2R_c^2)}\right) \frac{1}{Rc} & r \leq Rc \end{cases} \tag{2.3}$$

Rc is the Coulomb radius. $Z_{T,}$ Z_P called atomic charges of target and projectile respectively.

2.5.1.1 Wood Saxon Potential (WSP): For real and imaginary components of the nuclear optical potential, the volume Woods-Saxon form was used -

$$V_N(r) = \frac{-V0}{1+\exp(r-Rv)/av} + i \quad \frac{-W0}{1+\exp(r-Rw)/aw} \tag{3.4}$$

Where V_0 and W_0 are the potential depths, rv and rv are the radii, and av and aw are the diffuseness of the real and imaginary parts of the potential, respectively. $Rv=r_v(A_P^{(1/3)} + A_T^{(1/3)})$ and $Rw=r_w(A_P^{(1/3)} + A_T^{(1/3)})$. Thus, there are total of six parameters that needed to vary for obtaining the optimum value from the fitted data. Moreover, spin dependent terms can also be added as per the requirement of the problem in equation (2).

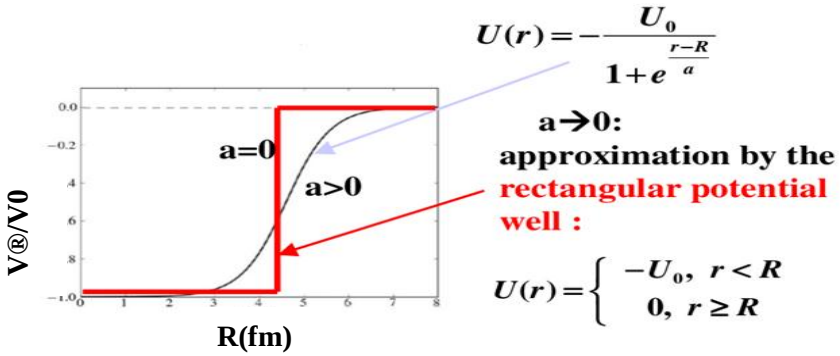

Figure 2.6: *Illustrative example of the form of Wood-Saxon potential.*

2.5.1.2 Sao Paulo Potential (SPP SPP construction considers the following building blocks,

(1) Both potential parts of optical potential are calculated in context of substantial systemization on nuclear densities. In the process, the parts were considered to have the same radial shapes.

(2) Energy dependence of bare potential is determined by a model on the basis of the nonlocal nature of the interaction. The bare interaction V_N entangles Pauli nonlocality and is correlated by folding potential V_F as follows [9],

$$V_N(R,E) \approx V_F(R) \exp \frac{-4v^2}{c^2}, \quad (2.5)$$

In this equation, v is local relative velocity among interacting nuclei. For speed of light in a vacuum c is shown. The Pauli nonlocality basically involves exchange of nucleons among target and projectile [10].

$$v^2(R,E) = \left(\frac{2}{\mu}\right)[E - V_C - V_N(R,E)] \quad (2.6)$$

V_C is the Coulomb interaction. μ is the reduced mass.

Folding potential V_F is given by,

$$V_F® = \int \rho_1(r_1)\rho_2(r_2)V(R - r_1 - r_2)dr_1dr_2 \quad (2.7)$$

The folding potential is calculated using nuclear matter distributions that account for the nucleon's limited size and a zero-range approach to nucleon-nucleon interaction V (r).

A systematization of nuclear densities was created for generating a universal parameter-free explanation of nuclear interaction by a thorough investigation that included the extraction of charge distributions. This charge distribution can be experimentally derived from electron scattering data. The Dirac-Hartree-Bogoliubov model calculates theoretical densities which use the 2-parameter Fermi (2pF) distribution for representing nuclear densities.

Here imaginary part is supposed to exhibit same shape as that of real component, incorporating an adjustable parameter N_i,

$$W(R, E) = Ni\ V_N(R, E) \tag{2.8}$$

For more than 30 systems, Ni was found to be well fitted with elastic scattering angular distribution data with an average value Ni= 0.78.

In general, the SPP can be written in a normalized form as below:

$$V_{SPP}(R, E) = (N_R(E) + i\ N_I(E))\ V_N(R, E) \tag{2.9}$$

$N_R(E)$ and $N_I(E)$ are energy dependent normalization factors look after Dynamic Polarization Potential (DPP). Further, it can be mentioned here that real and imaginary components of all DPP are dispersive and related by dispersion relation.

2.5.2 Microscopic Double Folding Model

A Schrödinger equation with an optical potential U® for two nuclei a+A can be written as

$$\left[-\frac{\hbar^2}{2\mu_\alpha} \nabla^2 + U(R) \right] \chi(\boldsymbol{R}) = E\, \chi(\boldsymbol{R}), \tag{2.10}$$

Where , E is center of mass energy for relative motion, R is center of mass distance μ_α is the reduced mass of two nuclei and, solution χ® indicates to elastic scattering of a + A with proper boundary conditions. A standard way of making eq. (1) describing elastic scattering is to expand total wave function of system a + A in terms of internal eigenstates of separate nuclei,

$$\Psi \alpha = \Sigma \psi_{ai} \psi_{Ai} \chi_{ij}®, \qquad (2.11)$$

χ_{ij}® describes the relative motion of internal states i and j. χ_{00} then signifies elastic scattering as i,j=0 gives the ground state. For the moment, if the effects of antisymmetrization between the two nuclei are ignored then U_{op} has the form

$$\begin{aligned} U_{op} &= V_{00} + \sum_{\alpha\alpha'} V_{0\alpha}\left(\frac{1}{E - H + i\varepsilon}\right)_{\alpha\alpha'} V_{\alpha'0} \\ &= U_F + \Delta U, \text{ say,} \end{aligned} \qquad (2.12)$$

Where V has the interaction between a and A and the sum is for all exited states of a or A. The first term is real and so called Folded Potential,

$$U_F(R) = V_{00} \equiv (\psi_{a0}\psi_{A0}|V|\psi_{a0}\psi_{A0}), \qquad (2.13)$$

Now if V is a local two body operator then

$$V = \Sigma v_{ij}$$

Where i is no of nucleon in one nucleus and j in the other. The folded potential (4) may be written as

$$U_F(R) = \int dr_1 \int dr_2 \, \rho_1(r_1)\rho_2(r_2)V(R + r_2 - r_1) \qquad (2.14)$$

Here ρi is the distribution of centers of mass of nucleons in ground state of the i^{th} nucleus (called density distribution) whose coordinates are defined by figure 2.7. The details of the double folding model are given in reference [11]

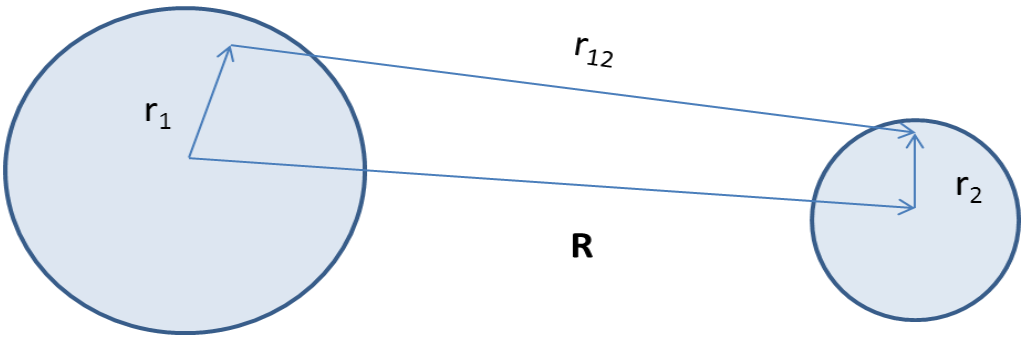

Figure 2.7: There is integration over two densities and therefore it is called the double folding model.

2.5.3 Dispersion Relation Calculation:

Real V(r, E) and imaginary W(r, E) potential parameters show an abrupt behavior in proximity of the Coulomb barrier and this is the consequence of optical model outcome from angular distribution of elastic scattering. Thus, dispersion relation analysis possesses its practical

implementation in the interpretation of energy dependence of these parameters at that region. If optical potential is of the form,

$$U(r,E) = V(r,E) + i\,W(r,E) \tag{2.15}$$

For energy below the barrier, the imaginary portion rapidly falls, and this event is accompanied by a rise in the real part. The threshold anomaly (TA) associated with this behaviour was part of the investigation for strong bound projectiles. [12]. Dispersion interrelates real (V(r, E)) and imaginary (W (r, E)) components as follows,

$$\Delta V(r,E) = \frac{P}{\pi}\int_0^{\infty} \frac{W(r,E')}{E'-E}\, dE' \tag{2.16}$$

This equation provides the potential at a given radial distance. Here, P is the principle value and ΔV (r, E) depends on energy. As the nuclear forces are due to the continuous interchanging of particles thus potentials are non-local in nature. The real potential can be better represented as follows**.** The above equation shows that W (r, E') causes variation in value of ΔV (r, E) every energy but as W is not precise, the value of ΔV (r, E) is also not fixed in the process. Thus the real part can be given as-

$$V(r,E) = V_0(r,E) + \Delta V(r,E) \tag{2.17}$$

The very popular method for real part calculation is a linear schematic model for potential parameter energy dependence. Following this, V(r, E) is made up of three linear segments of W(r, E) as in figure 2.8

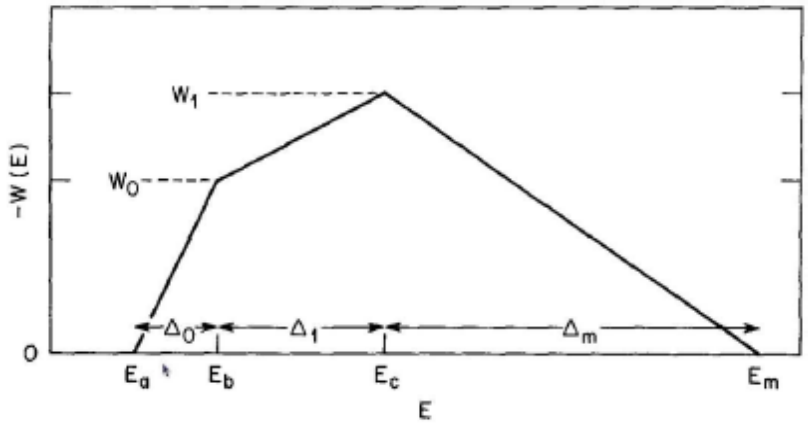

Figure 2.8: *The liner segments of W(r, E). The figure is taken from reference [13].*

The algebraic equation for the ΔV (r, E) will be

$$\Delta V(E) = (E-E_b)\frac{P}{\pi}\int_0^{\infty}\frac{W(E')}{(E'-Eb)(E'-E)}\,dE' \qquad (2.18)$$

E_b should be taken as reference energy. For one more reference energy Es, ΔV (E) will be,

$$\Delta V_{Es}(E) = \Delta V(E) - \Delta V(Es) \qquad (2.19)$$

ΔV(E) makes contribution from small increments (Wij=W(Ei)-W(Ej)) of each line segment,

$$\Delta Vij(E)=\frac{Wij}{\pi}\,[\varepsilon_i ln|\varepsilon_i| - \varepsilon_j ln|\varepsilon_j|\,], \qquad (2.20)$$

Here, $\varepsilon_i = \frac{(E-Ei)}{\Delta ij}$, $\varepsilon_j = \frac{(E-Ej)}{\Delta ij}$ and $\Delta ij = (Ej-Ei)$.

The resultant real part thus come out to be,

$$\pi\Delta V(E) = W_0[\varepsilon_a ln|\varepsilon_a| - \varepsilon_b ln|\varepsilon_b|\,] + (W_1-W_0)\,[\varepsilon'_b ln|\varepsilon'_i| - \varepsilon'_c ln|\varepsilon'_c|\,] - W1[\varepsilon''_c ln|\varepsilon''_c| -$$

$$\varepsilon''_m ln|\varepsilon''_m|\ ],+\ W_1[\eta\ ln\ \eta-(\eta+1)\ ln\ (\eta+1)] \quad (2.21)$$

Where, W_0, $W_1 \geq 0$ and $\varepsilon_i = \frac{(E-E1)}{\Delta 0}$, $\varepsilon'_i = \frac{(E-Ei)}{\Delta 1}$, $\varepsilon''_i = \frac{(E-Ei)}{\Delta m}$, $\eta = \frac{\Delta 1}{\Delta m}$

2.5.4 Coupled Channel Calculation:

When a projectile approaches a target nucleus in a laboratory frame, the interaction between them can result in a number of possible channels. During the process, some rearrangements can also play a variety of roles. The coupled channel calculations basically predict the effect of these multistep process. As we have discussed earlier that depending on the time scale we can always categorize the reaction as direct or compound. We will be elaborating on the direct reaction process for this modeling. The calculations involving bound inelastic states without transfer or breakup in the account are simple coupled channel calculations The influence of transfer in different partitions makes it Coupled reaction Channel (CRC). If breakup channels are incorporated from continuum with energy/momentum discretization then the adopted method is Continuum Discretized Coupled Channel (CDCC) calculations. We executed CRC and CDCC calculations for the vivid theoretical discussion of various channels using the code FRESCO [14].

2.5.4.1 CRC

During the process of nuclear reaction, several possible channels may contribute. Every reaction channel may be represented by a basis state and total wave function is consequence of superposition of all these bases as below-

$$|\Psi_{tot}>= \sum_{i=1}^{N} ai|\psi i> | \quad (2.22)$$

Now as total wave function space is associated with both direct and compound nuclear parts but our focus is on the direct reaction part and therefore, a projection of complete wave function has to be drawn on direct reaction space. Thus if a projection operator is applied to the total wave function onto the model space then

$$\hat{P}|\Psi_{tot}>= |\Psi>= \sum_{i=1}^{N} a_i|\phi_i(\zeta)\chi_i(\vec{R})> \quad (2.23)$$

where |φi >=|φipφit >, φit and φip are the states (bound or continuum) of target and projectile for i^{th} channel and χi represents the wave-function depending on the relative separation between them for that channel.

In model space, a complete Hamiltonian Ħ and total energy E, Schrödinger equation

[Ħ-E] $|\Psi_{tot}>=0$ is converted to [H-E] $|\Psi_{tot}>=0$ with

$$H = P\text{ĦP} - \text{PĦQ}\frac{1}{Q\text{ĦQ}-\text{E}-\text{i}\epsilon}\ Q\text{ĦP} \quad (2.24)$$

Here Q=1-P, ϵ shows dropped channels possess time retarded propagator and thus removal of flux from model space. Thus second term as whole signifies the excluded channels. The model Hamiltonian H uses optical potential as effective potential with the usual meaning of real and imaginary incoming flux. The model Hamiltonian could now be individually on the basis states Φi. If Ei is kinetic energy in that channel then channel projected Hamiltonian H satisfies

$$H_i\text{-}E_i= <\Phi_i|\ H\ \text{-E}|\Phi_i> \quad (2.25)$$

The interaction potential Vi is defined to present in Ħ which is not included in Ħi, so

$$Ħi - Ei + Vi = H - E \qquad (2.26)$$

This gives vanishing diagonal matrix element $\langle \Phi_i | V | \Phi_i \rangle = 0$.

If we take the model Schrödinger equation $[H - E]\ \Psi = 0$ then its projection onto different basis states Φ, the set of equations become:

$$[Ei - Hi]\ \Psi i(Ri) = \Sigma \langle \Phi_i | H - E | \Phi_j \rangle\ \Psi j(Rj),\ i \neq j \qquad (2.27)$$

These equations couple together the unknown wave functions Ψi(Ri). The matrix element can be expended in the following different forms-

$$H - E = Hi - Ei + V \quad \text{(post form)}$$

$$= Hj - Ej + Vj \quad \text{(prior form)} \qquad (2.28)$$

Therefore,

$$\Phi_i | H - E | \Phi_j \rangle = V_{ij}^{post} + [H_i - E_i]\ K_{ij} \text{ (post)}$$

$$\text{Or} \qquad = V_{ij}^{prior} + K_{ij}[H_j - E_j] \text{ (prior)}$$

Where

$$V_{ij}^{post} \equiv \langle \Phi_i | V_i | \Phi_i \rangle\ ,\ \ V_{ij}^{prior} \equiv \langle \Phi_j | V_j | \Phi_j \rangle \qquad (2.29)$$

The overlap function $Kij = \langle \Phi_i | \Phi_j \rangle$ arises from non-orthogonality between two basis states Φ_i and Φ_j if these are in different mass partitions. More details are given in reference [14].

2.5.4.2 CDCC

The studies of breakup on cluster structure of exotic nuclei is a very interesting field of research nowadays. The phenomena of breakup become difficult to be tackled with perturbation due to multi-step effects. The Continuum discretized coupled channel approach is a non-perturbative method that treats breakup to all orders and incorporates Coulomb and nuclear effects on an equal footing (CDCC). According to our understanding of quantum physics, bound states are discrete, finite, and can be normalized, whereas unbound states are continuous, infinite, and can't be normalized. Thus to obtain the solution for these unbound states, the continuum should be replaced with a discretized continuum so that the wave-function suit to be normalized. We can achieve this task by (a) including continuum to Coupled channel calculation and (b) characterizing continuum as a finite set of square integrable states. Let's consider a reaction p+t → v+c+t here v and c stand for valance and core fragments after the breakup of a projectile and t, p are target, projectile respectively,.

Figure 2.9: *Represent the coordinates of arrangement and now the three body becomes two body.*

Hamiltonian of the system becomes,

$$H_{3b} = \hat{T}_r + \hat{T}_R + V_{vc} + V_{vt} + V_{ct} \quad (2.30)$$

Where initial who terms are kinetic energy operators and the other three are potential energy operators. As well as the three body wave function can be designated as a superposition of bound state wave function and integration of all the wave functions of continuum state up to infinity as follow

$$\Psi^{(1)}_{\vec{K}_0}(\vec{R}, \vec{r}) = \phi_0(\vec{r})\chi_0(\vec{R}) + \int d\vec{k}\, \phi_{\vec{k}}(\vec{r})\chi_{\vec{K}}(\vec{R}) \quad (2.31)$$

Here, $\underset{k}{\rightarrow}$ is the momentum of fragments (c+v) and $\underset{K}{\rightarrow}$ is the momentum of the target and projectile. The Schrödinger equation solution becomes impractical for such kind of situation and therefore discretization of the continuum wave function into finite discretized square integrable basis is mandatory. In the average method, the radial functions for the continuum bins $\tilde{u}_p(r)$, are a superposition of the scattering eigenstates within a bin $[k_{p-1}, k_p]$.

$$\tilde{u_p}(r) = \sqrt{\frac{2}{\pi N_p}} \int_{k_{p-1}}^{k_p} w_p(k) u_k(r) dk \quad (2.32)$$

Here, $\omega_p(k)$ is the weight function, Np is the normalization constant selected such that $\tilde{u}_p(r)$ form an orthonormal set, while p=0 bound state and p ≥ 1excited states. $\omega_p(k)$ is the weight function. The total wave function, s the function of every single bin will be

$$\Psi(\vec{R},\vec{r}) = \sum_{p=0}^{N} \tilde{\phi}_p(\vec{r})\chi_p(\vec{R}) \tag{2.33}$$

Now, the Schrödinger wave function can be solved and obtain the S-matrix elements by utilizing partial wave decomposition and proper boundary conditions. These S-matrix components may be utilized for calculating the cross-section of exclusive breakup channels. Thus this described method of CDCC calculations is adopted in the theoretical analysis in the present thesis. More elaborating detailing on the topic is covered in reference [14].

References

[1] THES, Ali, Asif, 2016/03/23, Excitation Function Studies of Some Nuclear Reactions in 18O+175Lu System.

[2] T. Banerjee, et al., Vacuum 144 (2017) 190-198

[3] C. Joshi, A. S. D. Kabiraj, H. Kumawat, and N. Singh, Proceedings of the DAE Symp. on Nucl. Phys. 63 (2018).

[4] H. Bethe und J. Ashkin in ”Experimental Nuclear Physics, ed. E. Segr, J. Wiley, New York, 1953, p. 253.

[5] W. R. Leo, Techniques for Nuclear and Particle Physics - A How-to Approach

(Narosa PublishingHouse, 1987).

[6] A. Chatterjee. *LAMPS*. –. URL http://www.tifr.res.in/pell/lamps.html.

[7] N Keeley *et al*, *Prog. Part. Nucl. Phys.* **59**, 579 (2007).

[8] A Mukherjee, U Datta Pramanik, S Chattopadhyay, M Saha Sarkar, A Goswami, P Basu, S Bhattacharya, M L Chatterjee and B Dasmahapatra, *Nucl. Phys. A* **635**, 305 (1998)

[9] J. M. Figueira,∗ D. Abriola, J. O. Fern´andez Niello, A. Arazi, O. A. Capurro, E. de Barbar´a, G. V. Mart´ı,D. Mart´ınez Heimann, A. J. Pacheco, and J. E. Testoni, PHYSICAL REVIEW C 73, 054603 (2006)

[10] M. A. Cândido Ribeiro, L. C. Chamon, D. Pereira, M. S. Hussein, and D. Galetti, Phys. Rev. Lett. 78, 3270

[11] G.R. Satchler, W.G. Love, Phys. Rep. 55 (1979) 183.

[12] M.A. Nagarajan, C.C. Mahaux, G.R. Satchler, Phys. Rev. Lett. 54 (1985) 1136.

[13] C. Mahaux et al. *Nuclear Physics A*, 449:354, 19

[14] I. J. Thompson and Filomena M. Nunes. Cambridge University press New York, USA, 2009.